

Modifications to Model IV Fluid Catalytic Cracking Units to Improve Dynamic Performance

Iftikhar Huq and Manfred Morari

Chemical Engineering, 210-41, California Institute of Technology, Pasadena, CA 91125

Ronald C. Sorensen

Chevron Research and Technology Co., Richmond, CA 94802

Model IV fluid catalytic cracking units (FCCUs) differ from other cracking units in that model IV FCCUs do not have slide valves in the catalyst circulation lines to enable direct control of catalyst circulation rate through the unit. Reducing fluctuations in catalyst circulation rate is found to significantly improve closed-loop performance of the FCCU. Some design and operational modifications that can be made to model IV FCCUs to improve closed-loop performance at the regulatory level based on this insight are modeled and compared. Closed-loop performance of a model IV FCCU operated with the weir and standpipe always flooded is examined. The achievable performance is significantly better than that of the standard model IV FCCU. The closed-loop performance of the model IV FCCU modified to incorporate slide valves in the catalyst circulation lines is also examined. The performance of the FCCU with slide valves is better than the performance achievable by the FCCU with the weir flooded. It is found that model IV FCCUs are ill-conditioned owing to the use of the weir and standpipe arrangement in the regenerator section. Both the operational and design modifications studied reduce plant ill-conditioning appreciably.

Introduction

The fluid catalytic cracking process is used to crack high boiling gas oil fractions into a range of lighter hydrocarbons of which gasoline is the most valuable. The distinguishing feature of a model IV fluid catalytic cracking unit (FCCU) is that there is no direct control of catalyst circulation rate between the reactor and regenerator. Only indirect control is possible by varying the driving force for catalyst flow.

The FCCU operates as follows (Figure 1). Fresh feed is contacted with hot catalyst at the base of the riser (Figure 1) and travels rapidly up the riser where the cracking reactions occur. The desirable products of the reaction are gaseous hydrocarbons which are passed to a fractionator and subsequently to separation units for recovery and purification. The undesirable byproduct of cracking is coke which is deposited on the catalyst particles, reducing their activity. A catalyst coated with coke is called *spent catalyst*, and is transported to the regenerator section where the coke is burned off, thereby restoring catalytic activity and raising catalyst temperature.

The regenerated catalyst is transported to the riser base where it is contacted with more fresh feed. Regenerated catalyst at the elevated temperature provides the enthalpy required to vaporize the fresh feed as well as the energy required for the endothermic cracking reactions.

Fundamental modeling work on FCCUs has been reported by Lee and Groves (1985), Felipe (1992), Kurihara (1967), and McFarlane et al. (1993). All the models except the one by McFarlane et al. (1993) assume that the FCCU is equipped with slide valves to control catalyst circulation rate. Elnashaie and El-Hennawi (1979) developed a steady-state model of a model IV FCCU and later extended it to include dynamics (Elnashaie and Elshishini, 1992). Several control studies on FCCUs with slide valves have been reported. A sample of recent control studies on FCCUs include the works by Hovd and Skogestad (1993), Grosdidier et al. (1993), Monge and Georgakis (1987), and Arbel et al. (1993). The preceding list of authors is by no means exhaustive, but for continuity of presentation, we will not digress into a more detailed literature survey.

Correspondence concerning this article should be addressed to M. Morari.

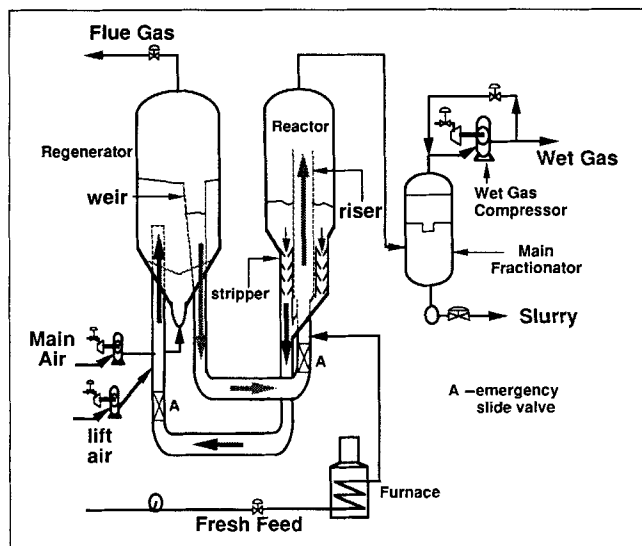


Figure 1. Model IV FCCU schematic.

The model developed by McFarlane et al. (1993) was selected for this study since it provides a comprehensive description of both the reactor and regenerator. Although the riser model is very simple, it provides sufficient information for regulatory control studies. Furthermore, the catalyst flow interactions between the reactor and regenerator are accounted for. Catalyst flow interactions between the reactor and regenerator sections are not addressed in any of the other models. This model is currently also used for educational purposes at Lehigh University (Kalra et al., 1993). While a specific model is used for this study, the conclusions are explained qualitatively on physical grounds. Therefore, the results are believed to be generic to model IV FCCU operation.

The economically optimal and safe operation of a processing unit requires that the unit is designed appropriately:

- From a steady-state point of view
- From a dynamic point of view, in that it is possible to run the unit at the desirable operating conditions despite dynamic variations in the environment, for example, disturbances, feedstock changes, or drifts in the parameters defining the operation of the unit.

The work described in this article is focused on this second aspect of the design process. Design and operational modifications that can be made to model IV FCCUs to improve closed-loop dynamic performance are examined.

Motivation

The observed closed-loop response of any given processing unit might be acceptable or unacceptable when evaluated by appropriate criteria. If the performance is acceptable, then there might be little incentive to improve the overall process. If the observed performance is unacceptable, however, then a natural question is whether one can obtain better performance. Note that the dynamic operability of the plant depends on two factors: the design of the unit itself and the design of the associated control system. Thus, the poor performance must be due to one (or both) of the following two causes:

Control System Deficiencies. The controller might be poorly tuned. The controller structure is inappropriate for the process under study. An example might be if single-loop controllers are used when multivariable controllers would provide much better control (for example, for ill-conditioned plants).

Plant Design Deficiencies. The physical design or setup of some part of the overall plant prevents one from achieving better closed-loop performance.

Clearly if it can be shown that regardless of the controller chosen, one cannot achieve acceptable closed-loop performance, then there must be some feature of the plant design itself that prevents good control. In general, it is not easy to rigorously establish that no controller will improve the observed performance of the process under study. A simplified approach that utilizes currently available theory has to be undertaken to assess the best closed-loop performance achievable from a given plant.

The following measures have been used in this article to examine *qualitatively* possible physical design limitations of the plant itself:

- Right half-plane transmission zeros (RHPT zeros) within the desired bandwidth will limit achievable closed-loop performance of the process regardless of the controller type used (Holt and Morari, 1985; Morari et al., 1987). Several of the control structures formulated have significant RHPT zeros, that is, RHPT zeros within the desired bandwidth.
- The model by McFarlane et al. (1993) indicates that the model IV FCCU is ill-conditioned, that is, plant gain is strongly dependent on the input direction. Ill-conditioned plants are characterized by strong directionality, that is, inputs in the direction of high plant gain are strongly amplified, while inputs in the direction of low plant gain are not (Morari and Zafiriou, 1989; Skogestad et al., 1988).

To obtain a more *quantitative* measure of achievable performance, we will use the structured singular value (commonly referred to as μ). The properties of μ -synthesis (μ -optimal controller design) and μ -analysis that we will appeal to are the following:

- Model uncertainty is always present in practice. μ -synthesis explicitly accounts for model uncertainty during controller synthesis. The subsequent analysis also accounts explicitly for uncertainty.
- No restrictions are imposed on controller structure during μ -synthesis. In general the μ -optimal controller will be multivariable. Note that it is most common to use single-loop PI (or PID) controllers at the regulatory level. It is clear that using PI (or PID) controllers restricts controller structure. The major goal in this article, however, is to determine the best possible performance regardless of what controller is used. Thus the best achievable performance with any controller would be just as good or better than that achievable with PI (or PID) controllers.
- A wide range of disturbance signals are considered when designing the μ -optimal controller. For an appropriately scaled system (Eqs. 1, 2, 3) all disturbances satisfying $\|\hat{d}\|_2 \leq 1$ are considered. The μ -optimal controller minimizes the largest possible gain which can result from any \hat{d} satisfying $\|\hat{d}\|_2 \leq 1$.

- Robust stability and robust performance can be addressed in a rigorous and consistent manner.
- For a fixed uncertainty and performance specification (to be discussed shortly), robust performance guaranteed $\Leftrightarrow \mu_{RP}(\omega) < 1$ for all ω .
- In comparing different designs using a fixed uncertainty and performance specification, the lower the $\mu_{RP}(\omega)$ for a given design, the better the design is.

In this article the best possible performance of the model IV FCCU is assessed. Subsequently, design and operational modifications that can be implemented on the model IV FCCU to improve dynamic performance are proposed. The best closed-loop performance attainable *after* implementing these modifications is compared to the best performance obtained from the original model IV FCCU to assess whether the proposed modifications in fact result in better plant designs.

Preliminaries

The operating points used for the simulations are tabulated in Appendix A. In order to facilitate easy comparisons of different inputs, outputs, and disturbances, the system was made dimensionless as follows:

$$\hat{y} = y_{\text{scale}}^{-1}(y_{\text{dim}} - y_{ss}) \quad (1)$$

$$\hat{u} = u_{\text{scale}}^{-1}(u_{\text{dim}} - u_{ss}) \quad (2)$$

$$\hat{d} = d_{\text{scale}}^{-1}(d_{\text{dim}} - d_{ss}). \quad (3)$$

The scaling factors used to scale the inputs and outputs are tabulated in Appendix A as well. Note that \hat{u} , \hat{y} , and \hat{d} are vectors since we have a multiple input/multiple output (MIMO) system, and at the *nominal* operating point the inputs, disturbances and outputs are all zero vectors. Furthermore \hat{y} is the output error vector. Each element of the input vector \hat{u} is scaled so that all physically implementable manipulated variable inputs are of magnitude less than one. The output error vector is scaled to make each error element equally significant to the process. The modeled disturbances to the system are:

1. d_1 —Variations in ambient temperature.
2. d_2 —Changes in feed coking characteristics resulting from variations in feed quality.
3. d_3 —Pressure fluctuations propagating back from the main fractionator to the reactor section of the FCCU.

An additional disturbance often cited in the literature (Hovd and Skogestad, 1993; Lee and Groves, 1985) is variations in inlet feed temperature. Here it is assumed that feed temperature is maintained at a prespecified setpoint by a local temperature controller and is therefore not considered a disturbance to the system.

Variations in ambient temperature affect compressor throughput and therefore the ability to burn off coke deposited on the catalyst particles. High ambient temperatures lead to lower oxygen supply to the regenerator and reduce the amount of coke that can be burned off (and therefore the fresh feed rate that can be processed). Feed quality refers to the coking characteristics of incoming feed, that is, how much coke will be deposited on the catalyst particles after comple-

tion of the cracking reaction. Changes in feed quality are reported to be a significant process disturbance (Grosdidier et al., 1993; Hovd and Skogestad, 1993; McFarlane et al., 1993), as it directly affects the coke deposition rate on the catalyst and therefore the feed processing rate. A number of process disturbances (including changes in feed quality) eventually affect reactor pressure. Of significance are fluctuations in the main fractionator pressure that affect reactor pressure. Changes in the main fractionator pressure can arise when vapor flow rate is altered (such as a result of changes in wet gas compressor suction flow rate). Variations in internal vapor and liquid traffic in the main fractionator (due to the changes in the condenser/reboiler duty) can also lead to changes in the main fractionator pressure. In the original model a constant pressure drop between the main fractionator and reactor section of 9.5 psi (65 kPa) (ΔP_{frac}) was assumed. Fluctuations in fractionator pressure can be effectively modeled as variations in ΔP_{frac} . Pressure disturbances in downstream recovery units (downstream from wet gas compressor) can also be effectively modeled as changes in ΔP_{frac} .

Variations in ambient temperature (which affects compressor throughput) were modeled as ramps with a period of 24 hours. The designed controllers were capable of rejecting disturbances in ambient temperature rapidly. Fluctuations in feed quality (disturbance d_2) were modeled as steps because the fresh feed composition in the feed holdup tank changes rapidly when heavy oil cuts of different compositions are added. Since pressure fluctuations in the reactor are expected to occur on time scales of tens of seconds, the fluctuations were modeled as steps. The “typical” peak deviation assumed for changes in ΔP_{frac} is tabulated in Appendix A. Each disturbance is scaled by its maximum expected deviation from steady state. Thus any disturbance input vector element of magnitude one represents the largest (smallest) expected disturbance. Nominal values for the disturbances and corresponding scaling factors are tabulated in Appendix A.

In this article both design and operational modifications to model IV FCCUs are studied. For notational convenience different modifications to the original model are referred to as model B and model C (this notation will be explicitly stated as required). Model A refers to the original model IV FCCU. The control schemes considered in this study are listed in Table 1.

The output variables are the same for all control schemes. Maintaining riser temperature (T_r) at a predetermined setpoint is critical to overall process economics, as it strongly affects product yield. It is necessary to maintain flue gas oxygen concentration ($C_{O_2,sg}$) above a prespecified minimum to prevent operation in the transitional zone between total combustion and partial combustion modes which is reported to be unstable (Arbel et al., 1993; Grosdidier et al., 1993). Lift

Table 1. Notation for Different Control Schemes

Notation	Controlled Variables	Manipulated Variables
SI	$C_{O_2,sg}, T_r$	V_{lift}, F_3
SII	$C_{O_2,sg}, T_r$	V_{lift}, V_{14}
SHI	$C_{O_2,sg}, T_r$	V_{lift}, T_2

air supply (determined by V_{lift}) is always a manipulated variable, as it is the only source of additional air supply to the regenerator (the combustion air blower is operated at full capacity). Other available manipulated variables, such as fresh feed rate (F_3), flue gas valve opening (V_{14}), and feed temperature (T_2) are examined in conjunction with V_{lift} . There are several other manipulated variables and many other possible output variables, and the most common of these will be discussed.

Combustion air supply is sometimes used as a manipulated variable. For maximum economic benefit of the investment made in the blower, however, the combustion air blower is operated close to maximum capacity. Therefore, changing the compressor speed does not result in appreciable changes in air flow rate. Combustion air supply is thus not used as a manipulated variable. This is consistent with industrial practice where the combustion air blower is operated close to maximum capacity, with the blower speed regulator operated manually. Wet gas compressor throughput is often used to regulate reactor pressure. Since it was intended to examine the effect of variations in reactor pressure on overall FCCU operation, the wet gas compressor throughput was not used as manipulated variable. The wet gas compressor is also operated near maximum capacity.

Regenerator dense bed temperature, regenerator cyclone temperature, and flue gas CO concentration are sometimes used as controlled variables (Hovd and Skogestad, 1993; Lee and Groves, Jr., 1985; McFarlane et al., 1993). Owing to the strong interaction between the reactor and regenerator sections, regenerator temperature and reactor riser temperature are closely related. Recall that riser temperature influences product yield and distribution and therefore plant economics. Regenerator temperature responds relatively slowly to process changes owing to the large thermal inertia of the regenerator section (Hovd and Skogestad, 1993). Therefore, riser temperature is generally the controlled variable. Similar arguments apply to flue gas CO and O_2 concentrations. Low concentrations of CO (ppm range) or excess O_2 in the flue gas line indicate total combustion operation. Energy is required to provide O_2 (air), however, and it is economically beneficial to have just enough excess of O_2 to ensure operation in the total combustion mode. Controlling CO concentration in the flue gas line would not guarantee minimal excess O_2 in the flue gas line. Therefore, O_2 concentration is generally selected as the controlled variable.

In total combustion operation with sufficient CO combustion promoter, there is relatively little afterburn in the regenerator catalyst disengaging zone and cyclone temperatures are well below the metallurgical limits. This is not the case for partial combustion operation where afterburn can raise cyclone temperatures close to the metallurgical limits. In partial combustion mode, cyclone temperatures must be controlled to prevent meltdowns. In total combustion mode with CO combustion promoter, the cyclone temperatures are only monitored to ensure safe operation. It is assumed that cyclone temperatures are well below the metallurgical limit since the FCCU is operated in total combustion mode.

Uncertainty and performance description

Our analysis is based on linear models derived by lineariz-

ing the nonlinear model around the operating point tabulated in Appendix A. The open-loop step responses to a 0.2 (scaled) step in feed coking characteristics for the linear and nonlinear models are compared in Appendix A. The frequency range of interest (expected closed-loop bandwidth) was taken to be 10^{-4} to 10^{-2} rad/s, which corresponds to process variations on time scales of minutes to hours. Note that for these time scales, the dynamic response of the linear and nonlinear models are close (Appendix A, Figure 22). Unless otherwise stated, the response plots are those observed with the linear model. The state-space models for several selected control schemes are listed in Appendix B.

Since our control objective is effective disturbance rejection, the μ -optimal controllers were designed to minimize the ∞ -norm of the weighted sensitivity function. Thus for each control scheme an optimal controller was synthesized and the closed-loop performance achievable with this controller examined. The controllers were synthesized using software available in the μ -Analysis and Synthesis Toolbox (Balas et al., 1991) in MATLAB. Excellent descriptions of the calculation, interpretation, and use of μ are given in Balas et al. (1991) and Morari and Zafiriou (1989). A reasonable representation of model uncertainty is needed before the controllers can be synthesized. The uncertainty description adopted for this study will be discussed next. Note that unless explicitly stated, the analysis is carried out on the linearized models.

The model adopted for this study is only an approximate description of the actual FCCU process. In practice, model uncertainty is always present. An uncertainty model based on heuristic arguments has been adopted for this study. The formulation of the uncertainty model closely follows the procedure described in the μ -Analysis and Synthesis Toolbox (Balas et al., 1991), as well as the guidelines specified in Lundström et al. (1991). The uncertainty description postulated includes plant input and plant output uncertainty. The physical interpretation of these uncertainties are actuator uncertainty and measurement uncertainty, respectively. Clearly, the uncertainty level is dependent on frequency—it is difficult to accurately follow a rapidly changing signal while a slowly varying signal can be tracked relatively accurately. The block diagram used for closed-loop analysis is shown in Figure 2. At any frequency, the actual uncertainty level is given by $|W_I|$ and $|W_O|$. The blocks Δ_I and Δ_O are transfer matrices. The structures of Δ_I and Δ_O are prespecified, but the actual transfer functions are unknown except that they are norm bounded:

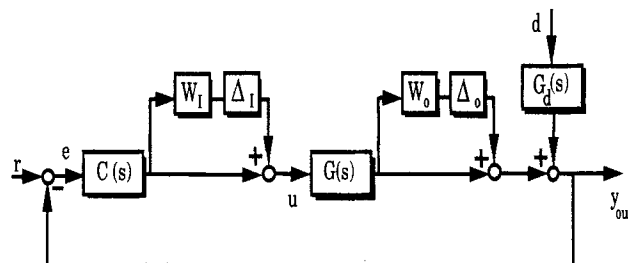


Figure 2. Closed-loop system.

Δ_I —Complex, diagonal; Δ_O —complex, full block. $\bar{\sigma}(\Delta_I) \leq 1$, $\bar{\sigma}(\Delta_O) \leq 1$.

$$\bar{\sigma}(\Delta_I) \leq 1 \quad \bar{\sigma}(\Delta_O) \leq 1. \quad (4)$$

The unknown transfer matrices Δ_I and Δ_O are used to parameterize the difference between the nominal plant $G(s)$ and the real plant, that is, the model uncertainty. The actual uncertainty level assumed is described below.

• **Input (Actuator) Uncertainty**—The inability of the process actuators to exactly follow the controller signal is accounted for explicitly. As mentioned before, actuators will be able to follow rapidly varying control signals only approximately, while slowly varying signals will be tracked relatively accurately. A low-frequency ($\omega < 10^{-3}$ rad/s) uncertainty of 5% was assumed in each input signal, increasing to 50% uncertainty at high frequency ($\omega > 10^{-1}$ rad/s). At even higher frequencies ($\omega \gg 10^{-1}$ rad/s) one can expect complete phase uncertainty (uncertainty $> 100\%$). Closed-loop robust performance analysis indicates that all the results hold even with more conservative uncertainty bounds (uncertainty level $> 50\%$ for $\omega > 10^{-1}$ rad/s). It is assumed that the actuators are independent of each other. The uncertainty in each input signal is therefore expected to be independent and Δ_I is assumed diagonal (no manipulated variable interactions). A magnitude/frequency plot for the uncertainty model in each input variable is shown in Figure 3. The transfer function used for the uncertainty description is

$$w_o = w_i = 0.05 \frac{129.515s + 1}{12.952s + 1} \quad (5)$$

$$W_I = w_i I \quad (6)$$

$$W_O = w_o I. \quad (7)$$

• **Output (Measurement) Uncertainty**—Owing to sensor limitations, the actual plant output may differ from what is measured. Uncertainty in each output signal was modeled in the same manner as input uncertainty, and W_O is assumed diagonal. It is more difficult to ascribe output uncertainty to sensor error only. Other factors including unmodeled plant dynamics may also contribute to output uncertainty. Such possible interactions between different output signals are accounted for by making Δ_O full block.

• **Performance Specification**—The control objective for all cases in this article is effective disturbance rejection. The performance requirements are:

1. high-frequency disturbance amplification by a factor of at most 2.5
2. steady-state offset of at most 0.5%.

The transfer function for the performance weights is:

$$w_p = 200 \frac{\frac{1}{\omega_p} s + 1}{\frac{500}{\omega_p} s + 1} \quad (8)$$

$$W_P = w_p I. \quad (9)$$

The performance requirement for each output variable was assumed to be the same. This is justified since the output variables were scaled so that any output error was equally

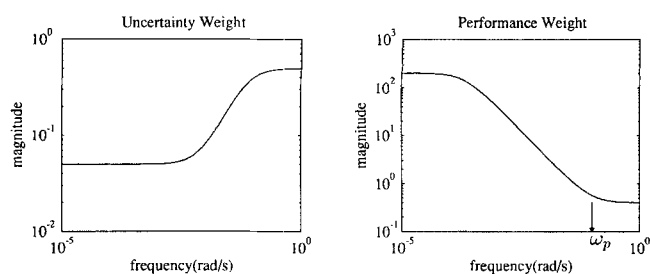


Figure 3. Uncertainty and performance specifications.

$$\omega_p = 0.1 \text{ rad/s.}$$

significant. A magnitude/frequency plot for the performance weight is plotted in Figure 3. The “corner frequency” ω_p (Eq. 8) is used as an adjustable parameter to quantify the best achievable performance for a given control scheme. Higher ω_p (Figure 3) implies faster closed-loop response (Lundström et al., 1991).

Analysis of Model A (Original Model IV FCCU)

Open-loop analysis of model A

Figure 4 is a plot of the maximum and minimum singular values of the plants corresponding to control schemes SI, SII, and SIII as a function of frequency. The maximum singular value of the disturbance transfer function matrix ($\bar{\sigma}(G_d)$) is also plotted. Note that the maximum plant gain for scheme SI is smaller than the maximum disturbance gain suggesting that the available control action might be insufficient to reject disturbances.

Catalyst flow behavior between the reactor and regenerator section is an important operational parameter in FCCU operation. Figure 5 gives the open-loop change in catalyst circulation rate at steady state as a function of change in reactor pressure. The nonlinear model was used to obtain the data in Figure 5. ΔP_{frac} was stepped up and the system allowed to attain steady state. The changes in catalyst circulation rate and reactor pressure were observed. Clearly increased reactor pressure leads to increased catalyst circulation rate at steady state, that is, there is a positive gain between changes in catalyst circulation rate and changes in reactor pressure.

The steady-state effect of a step increase in reactor (ΔP_r) on catalyst circulation rate is examined for model A. In particular we want to determine if the positive gain is generic for systems of this type or a consequence of the particular parameter choices. It is expected and our simulations show that

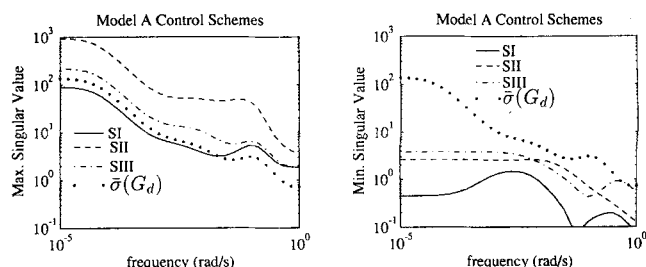


Figure 4. Frequency response plots for disturbance model and schemes SI, SII, and SIII, model A.

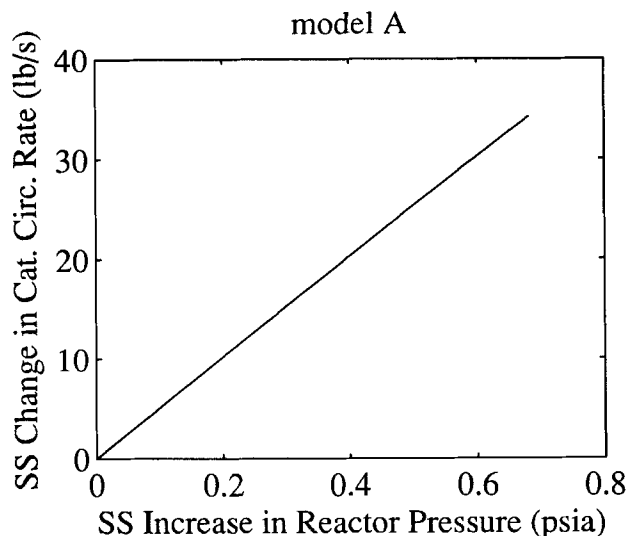


Figure 5. Dependence of catalyst circulation rate on changes in reactor pressure (ΔP_r) at steady state for model A.

positive ΔP_r results in a shift of catalyst from the reactor to the regenerator section. To explain the positive gain, the following question is posed for each catalyst U-bend: How much catalyst must be transferred from the reactor to regenerator to exactly counterbalance the increased reactor pressure so that there is no change in catalyst driving force in that U-bend at steady state? The independent variable is clearly ΔP_r and the dependent variable is taken to be the decrease in catalyst level in the reactor (ΔH_{str}), which is a measure of how much catalyst has been transferred. By deriving the requisite relations for the regenerated and spent catalyst U-bends it is possible to determine conditions under which the steady-state catalyst circulation rate will increase or decrease for a ΔP_r increase in reactor pressure. These bounds are derived below for model A.

Of the total amount of catalyst shifted from the reactor to the regenerator section, a fraction ends up in the standpipe (at steady state) and the remainder in the regenerator dense bed. The split is accounted for by defining a parameter α as follows:

$$\alpha = \frac{\Delta W_{sp}}{\Delta W_{str}} \quad (10)$$

The condition for net increase in regenerated catalyst flow rate at steady state for step increase in ΔP_r is

$$\frac{\Delta H_{str}}{\Delta P_r} > \frac{1}{\alpha} \frac{A_{sp}}{A_{str}} \frac{1}{\rho_c} \quad (11)$$

The condition for net increase in spent catalyst flow rate at steady state for a step increase in ΔP_r is

$$\frac{\Delta H_{str}}{\Delta P_r} < \frac{A_{reg}}{A_{reg} + (1 - \alpha) A_{str}} \frac{1}{\rho_c} \quad (12)$$

Table 2. Steady-State Plant Condition Number and Location of RHPT Zero for Model A Control Schemes

Scheme	Condition No.	RHPT Zero
SI	207	None
SII	363	0.273
SIII	59.4	None

Therefore, bounds on $\Delta H_{str}/\Delta P_r$ for which there will be a net increase in catalyst circulation rate at steady state for an increase in reactor pressure are

$$\frac{1}{\alpha} \frac{A_{sp}}{A_{str}} \frac{1}{\rho_c} < \frac{\Delta H_{str}}{\Delta P_r} < \frac{A_{reg}}{A_{reg} + (1 - \alpha) A_{str}} \frac{1}{\rho_c} \quad (13)$$

In model A α is close to one for all observed cases ($\alpha > 0.9$ typically). Thus after a process upset essentially all the catalyst shifted from the reactor to the regenerator section ends up in the standpipe once the system settles. Substituting $\alpha = 1$ in Eq. 13 yields:

$$\frac{A_{sp}}{A_{str}} \frac{1}{\rho_c} < \frac{\Delta H_{str}}{\Delta P_r} < \frac{1}{\rho_c} \quad (14)$$

Note that for $A_{sp} < A_{str}$ (as in model A) there will be an increase in catalyst circulation rate at steady state for an increase in reactor pressure.

The steady-state plant condition numbers as well as any RHPT zeros for model A schemes SI, SII, and SIII are summarized in Table 2. All three schemes are ill-conditioned, indicating that while nominal performance and robust stability might be satisfied, robust performance could be unsatisfactory (Morari and Zafiriou, 1989; Skogestad et al., 1988).

Closed-loop analysis of model A

Figure 6 is a plot of the robust performance $\mu(\mu_{RP})$ for model A control schemes SI, SII, and SIII. For all three cases

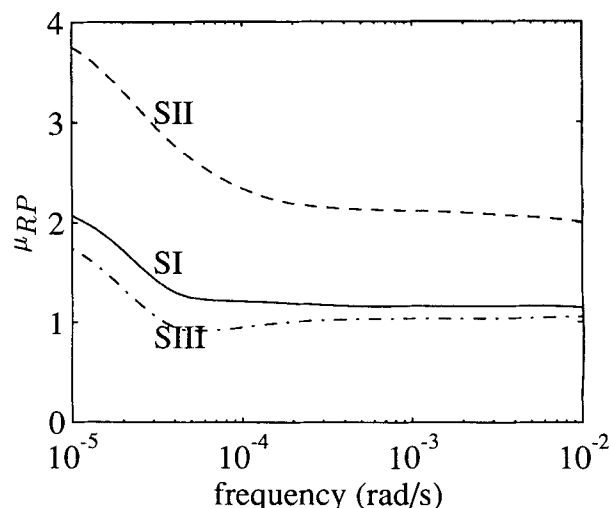


Figure 6. Robust performance comparison for model A, schemes SI, SII, and SIII, $\omega_p = 0.01$.

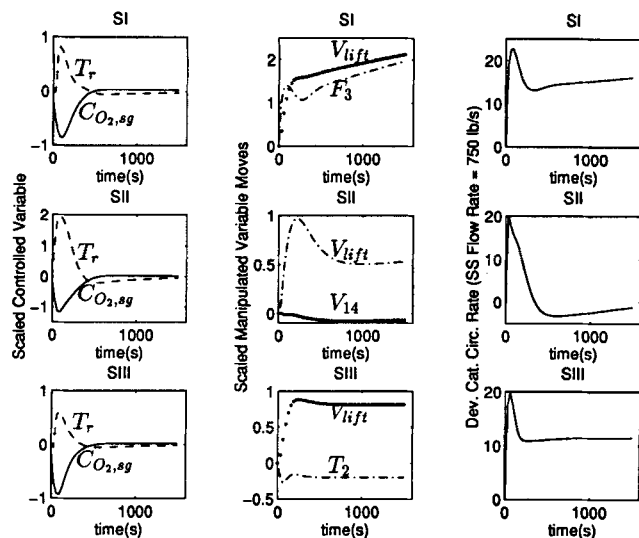


Figure 7. Closed-loop time response to unit step in fractionator pressure for model A schemes, $\omega_p = 0.01$ rad/s.

$\mu_{RP} > 1$ over the frequency range of interest, indicating that there are plants in the uncertainty set for which the designed controllers would be unable to provide the requisite performance. In all three cases, however, robust stability was achieved (plot not shown) and the closed-loop system would be stable for all allowable perturbations.

The time responses of model A schemes (nominal plants) to a unit step in ΔP_{frac} (disturbance d_3) are shown in Figure 7. Pressure upsets in downstream units propagating back to the FCC section are the most severe disturbances for this system. The other significant disturbance is variations in feed quality, but this disturbance eventually affects reactor pressure as well. In practice it is desirable to reject disturbances within about 10 to 15 min from the onset, and therefore $\omega_p = 0.01$ for all cases considered in model A. The controlled variables (Figure 7) display relatively large deviations from their steady-state values during the disturbance transient period. In addition it is not possible to reject a unit step disturbance in d_3 using scheme SI (more control action required than is available). Note that the transient deviations of the controlled variables from steady state are largest for scheme SII (largest μ_{RP} over frequency) and smallest for scheme SIII (smallest μ_{RP} over frequency).

Catalyst circulation rates are also observed to undergo large fluctuations (Figure 7). It is shown later that in open loop the deviation of output variables from steady state is directly related to the deviation of catalyst flow rate from steady state. Large fluctuations in controlled variables and catalyst flow rate are expected for model A owing to the use of an overflow weir and standpipe setup in the regenerator section which serves to convey regenerated catalyst to the riser. Regenerator dense bed catalyst is fluidized by passage of combustion air through it and flows over the weir into the standpipe (Figure 1). Since catalyst particles are small and the bed is fluidized, slight variations in regenerator bed height cause relatively large variations in catalyst flow rate over the weir. Furthermore, since the cross-sectional area of the standpipe is small compared to the cross-sectional area of the regenerator

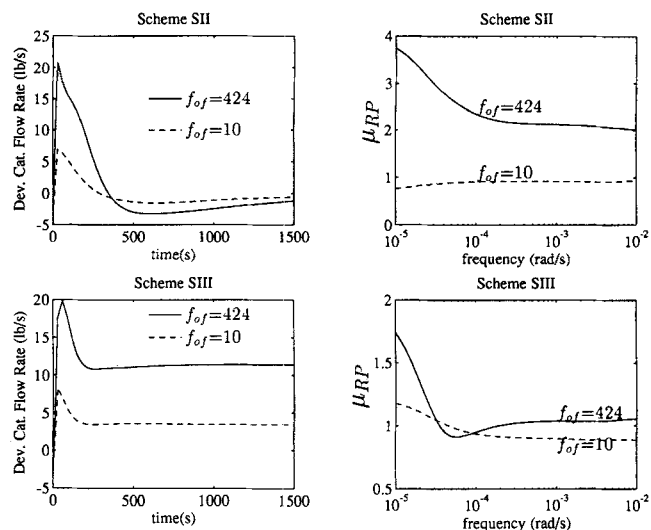


Figure 8. Comparison of time response and μ_{RP} for $f_{of} = 424$ and $f_{of} = 10$, model A, schemes SII and SIII, $\omega_p = 0.01$.

tor (7 ft² vs. 590 ft²), small variations in regenerator bed height will result in significant variations in standpipe inventory level and therefore regenerated catalyst flow rate. The equation governing catalyst flow over the weir is given by

$$F_{sp} = f_{of} \sqrt{A_{sp}} (z_{bed} - 13) + \beta \quad (15)$$

where f_{of} is the overflow factor. For a given standpipe area, f_{of} measures sensitivity of catalyst flow over the weir to changes in dense bed height. In the original problem formulation, this factor was 424. Small changes in dense bed height therefore result in relatively large changes in regenerated catalyst flow rate to the riser. Lowering f_{of} would be expected to reduce changes in flow rate over the weir and minimize variations in catalyst flow rate.

Figure 8 shows the closed-loop response of catalyst circulation rate to a unit step in fractionator pressure (disturbance d_3) for two different values of f_{of} as well as a μ_{RP} comparison for the two cases ($f_{of} = 424$ and $f_{of} = 10$). Two control schemes are considered—SII and SIII. The plant condition number as well as any RHPT zeros for schemes SII and SIII are tabulated in Table 3 for $f_{of} = 10$ and $f_{of} = 424$. Fluctuations in catalyst circulation rate are reduced by lowering f_{of} . Robust performance is also improved. To accomplish the reduction in f_{of} the constant factor β was adjusted to maintain F_{sp} constant for both runs while f_{of} was changed.

Table 3. Steady-State Condition Number and Location of Plant RHPT Zero(s) for Model A Schemes SII and SIII, for $f_{of} = 10$ and $f_{of} = 424$

f_{of}	SII		SIII	
	Condition No.	RHPT Zero	Condition No.	RHPT Zero
424	363	0.273	59.4	None
10	6.54	9.96×10^{-3}	4.23	None

It is evident that design or operational modifications made to model A to damp out fluctuations in catalyst flow rate are expected to improve closed-loop performance of the unit and reduce disturbance sensitivity. Physically it is difficult to reliably alter the overflow factor to reduce fluctuations in catalyst flow rate in model A. Two physically implementable modifications to model A are considered next.

Flooding the Weir and Standpipe in the Regenerator Section

The operational modification implemented in this study was to increase catalyst inventory and operate the regenerator section with catalyst level above the standpipe, thereby ensuring that the standpipe is always full, Figure 9. The operation of the rest of the unit remains unchanged. This operational modification could be implemented in practice by adding catalyst to the unit and then maintaining total catalyst inventory at the requisite level. We will refer to this unit as *model B*.

The primary difference between model A and model B is that model B is operated with the weir flooded and the standpipe always full. Therefore, the component of driving force due to catalyst level in the standpipe in model A is replaced with regenerator dense-bed height in model B. Several alternatives are available to compensate for the increased driving force due to additional catalyst head in the filled standpipe. For this study we reduced regenerator pressure and incorporated restrictions in the catalyst U-bends to generate additional pressure drop. The equation used to model the additional pressure drop is of the form:

$$\Delta P = \frac{1}{2} N \rho_c \frac{v^2}{g_c} \quad (16)$$

where

$N = N_{rgc} = 26$ for regenerated catalyst line,
 $N = N_{sc} = 22$ for spent catalyst line.

The additional pressure drop reduces overall driving force for both the regenerated catalyst flow and spent catalyst flow. N was used as an adjustable parameter to attain the desired pressure drop to maintain model B operating conditions within acceptable limits and close to the operating conditions in model A. Note the use of specific values for the number of velocity heads in the regenerated and spent catalyst lines in model B (Eq. 16). While actual quantitative results will vary somewhat with the selected values for N_{rgc} and N_{sc} , the observations and conclusions are unaffected by the selection. Figure 10 shows flow characteristic plots for different values of N_{rgc} and N_{sc} , including the case $N_{rgc} = N_{sc} = 0$, which corresponds to merely flooding the standpipe. In all cases the important flow characteristic, namely a negative gain between changes in reactor pressure and changes in catalyst circulation rate, is preserved.

Operating the FCCU as in model B should damp out fluctuations in catalyst circulation rate since relative changes in regenerator bed height are small owing to the large cross-sectional area of the regenerator section. It must be stressed that the critical modification made in model B is the flooding of the weir and standpipe.

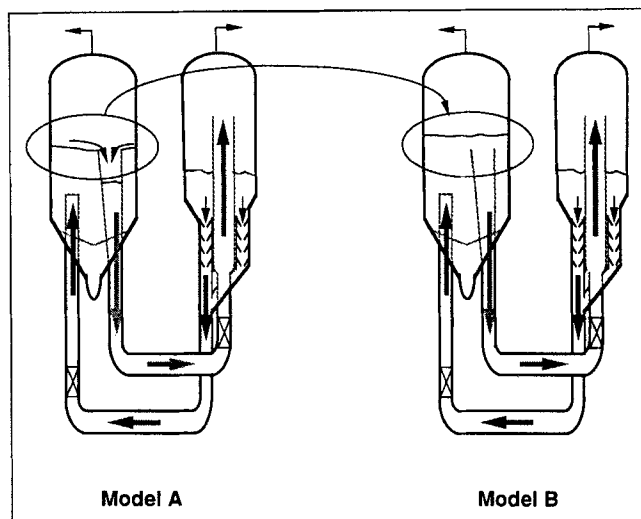


Figure 9. Operational modification to model A—weir flooded.

Open-loop analysis of model B

Figure 11 is a plot of the maximum and minimum singular values of the control schemes SI, SII, and SIII as a function of frequency. The maximum singular value of the disturbance transfer function matrix is also plotted. Note that as in model A the maximum plant gain for scheme SI is smaller than the maximum disturbance gain, suggesting possible manipulated variable constraint problems.

Catalyst flow characteristics for model B are different from those in model A. In model B increased reactor pressure results in decreased catalyst circulation rate at steady state, that is, *negative* gain between changes in catalyst flow rate and changes in reactor pressure (Figure 12). Figure 12 was obtained in the same manner as Figure 5.

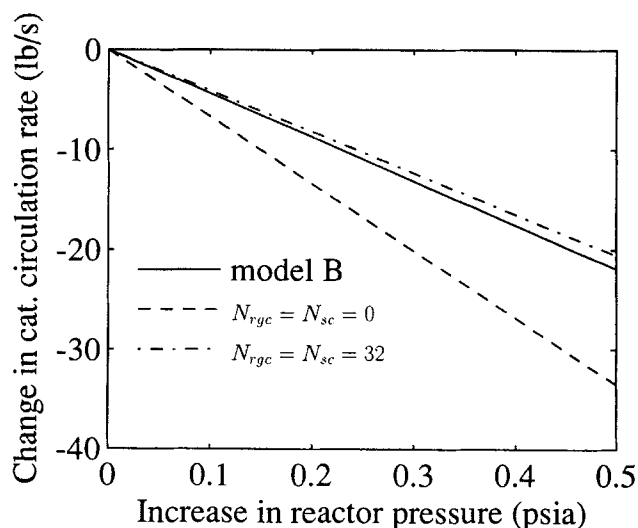


Figure 10. Catalyst flow sensitivity to reactor pressure for different N_{rgc} and N_{sc} in model-B-type setup.

For model B, $N_{rgc} = 26$, $N_{sc} = 22$.

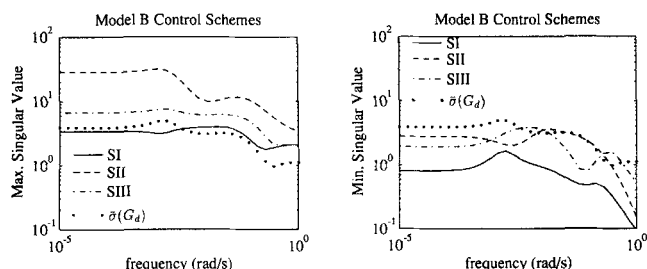


Figure 11. Frequency-response plots for disturbance model and schemes SI, SII, and SIII, model B.

Bounds similar to those for model A regarding the dependence of changes in catalyst circulation rate on changes in reactor pressure are derived for model B. Note that the parameter α described for model A does not apply to model B. To decrease regenerated catalyst flow rate at steady state for a step increase in ΔP_r we require

$$\frac{\Delta H_{str}}{\Delta P_r} < \frac{A_{reg}}{A_{str}} \frac{1}{\rho_c}. \quad (17)$$

To decrease spent catalyst flow rate at steady state for a step increase in ΔP_r we require

$$\frac{\Delta H_{str}}{\Delta P_r} > \frac{A_{reg}}{A_{reg} + A_{str}} \frac{1}{\rho_c}. \quad (18)$$

Combining these two conditions gives bounds on $\Delta H_{str}/\Delta P_r$ for which there will be a decrease in catalyst flow rate for an increase in reactor pressure:

$$\frac{A_{reg}}{A_{reg} + A_{str}} \frac{1}{\rho_c} < \frac{\Delta H_{str}}{\Delta P_r} < \frac{A_{reg}}{A_{str}} \frac{1}{\rho_c}. \quad (19)$$

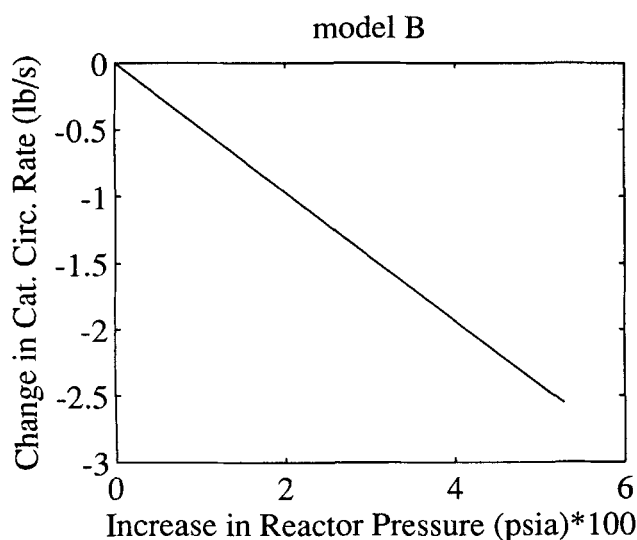


Figure 12. Dependence of catalyst circulation rate on changes in reactor pressure at steady state for model B.

Table 4. Steady-State Plant Condition Number and Location of RHPT Zero for Model B Control Schemes

Scheme	Condition No.	RHPT Zero
SI	4.22	2.86×10^{-3}
SII	10.2	$1.858 \pm i11.1$
SIII	3.51	1.762×10^{-3}

Clearly an increase in reactor pressure cannot possibly lead to an increase in catalyst circulation rate at steady state for model B regardless of the cross-sectional areas of any of the units (A_{sp} , A_{reg} , A_{str}). The bounds for model A which would result in a decrease in catalyst circulation rate are given by Eq. 13:

$$\frac{A_{reg}}{A_{reg} + (1 - \alpha) A_{str}} \frac{1}{\rho_c} < \frac{\Delta H_{str}}{\Delta P_r} < \frac{1}{\alpha} \frac{A_{sp}}{A_{str}} \frac{1}{\rho_c}. \quad (20)$$

By a suitably modified interpretation of α (for model B) the bounds for model A and model B can be shown to be similar. Note that A_{sp} in model A must be replaced by A_{reg} in model B.

The steady-state plant condition numbers as well as any RHPT zeros for model B schemes SI, SII, and SIII are summarized in Table 4. The steady-state plant condition numbers for model B schemes are much lower than the corresponding values for model A schemes. Control scheme SII has a RHPT zero outside the frequency range of interest and should not limit the achievable performance. Schemes SI and SIII, however, have RHPT zeros which are within the frequency range of operation and limit the achievable performance. $\mu_{RP} \approx 4$ for scheme SI and $\mu_{RP} \approx 7$ for scheme SIII. In rejecting unit-step disturbances, large overshoots in controlled variables were observed for schemes SI and SIII compared to scheme SII. The plots are not shown for brevity.

Closed-loop analysis for model B

Figure 13 is a μ_{RP} plot for model A scheme SII and model B scheme SII for identical uncertainty and performance specifications. Note that $\omega_p = 0.01$ for both cases, although model B can be expected to have faster closed-loop response. A μ -optimal controller was designed for model B that guaranteed robust performance, while the μ -optimal controller for model A could not guarantee desired performance given the expected uncertainties, disturbances, and performance requirements.

Figure 14 shows the closed-loop response of model B, control scheme SII to a unit-step disturbance in fractionator pressure. Compared to the closed-loop response for model A, scheme SII (Figure 7) the fluctuations in catalyst flow rate as well as controlled variable deviations from their steady-state values during the process transients are significantly reduced. Model B response is also faster than model A response. A significant improvement in closed-loop robust performance of the model IV FCCU is attainable simply by operating the unit as in model B. Physical justification for the improved performance of model B compared to model A will be discussed next in the context of the different flow characteristics of models A and B.

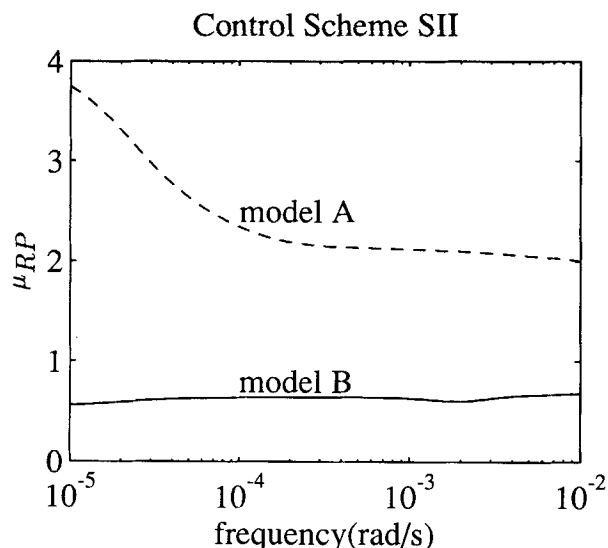


Figure 13. Robust performance comparison for model A and model B.
Identical uncertainty and performance specs. $\omega_p = 0.01$.

Comparison of Flow Characteristics for Models A and B

Figure 15 shows steady-state changes in catalyst flow rate as a function of increase in reactor pressure for models A and B. In addition to reactor pressure fluctuations, temperature variations in the reactor and regenerator also affect catalyst circulation rates as follows:

Regenerator. Variations in regenerator dense-bed temperature affect regenerator gas pressure. Regenerator temperature, however, does not change appreciably under normal conditions ($\pm 15^\circ\text{F}$) and regenerator gas volume is large. Regenerator gas-pressure changes are thus small and can be ignored.

Reactor Riser. Temperature variations in the reactor riser affect wet-gas production rate, which in turn affects reactor pressure.

Reactor temperature has the more significant effect on catalyst circulation rate. We show that due to the effect of temperature changes on catalyst circulation rate it is desirable to have a decrease in catalyst circulation rate at steady state for an increase in reactor pressure (negative gain be-

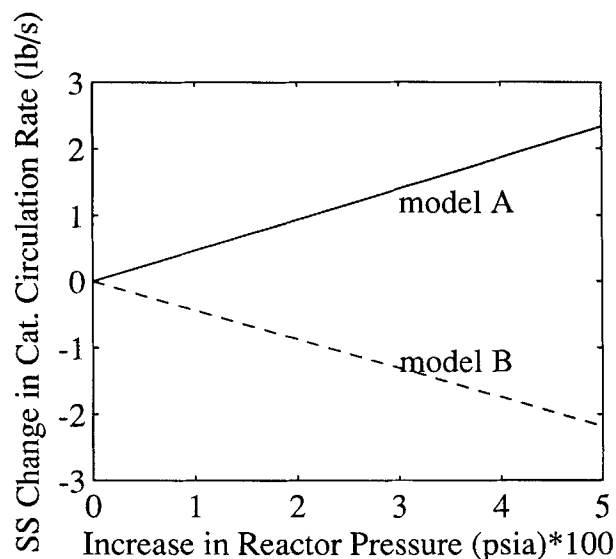


Figure 15. Steady-state variation in catalyst flow rate with increase in reactor pressure (nonlinear models).

tween reactor pressure changes and catalyst circulation rate changes).

Suppose an FCCU such as model A, where there is a positive gain between reactor pressure and catalyst circulation rate, is subjected to a disturbance which increases reactor pressure. Catalyst flow rate increases, elevating riser temperature. Increased riser temperature results in higher wet-gas production rate and yet higher reactor pressure. Steady state is reached when the net increase in driving force (due to pressure and catalyst head) is balanced by the additional pressure drop due to increased catalyst circulation rate. The effect of the disturbance is therefore amplified for FCCUs with positive gain between changes in reactor pressure and catalyst circulation rate.

The argument can be reversed for a setup like model B with a negative gain between changes in reactor pressure and changes in catalyst circulation rate. In model B the net effect of disturbances is reduced. This phenomenon is shown in Figure 16a, where the actual reactor pressure change at steady state is plotted as a function of change in ΔP_{frac} . The solid line is the expected reactor pressure change (ΔP_{frac}) in the absence of any other effects. The actual reactor pressure changes are larger than expected for model A and lower than

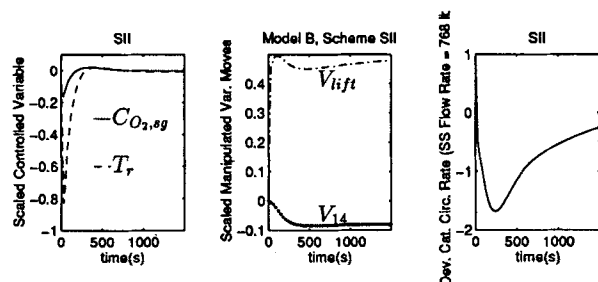


Figure 14. Closed-loop time response of model B, scheme SII to a unit step in ΔP_{frac} , $\omega_p = 0.01$.

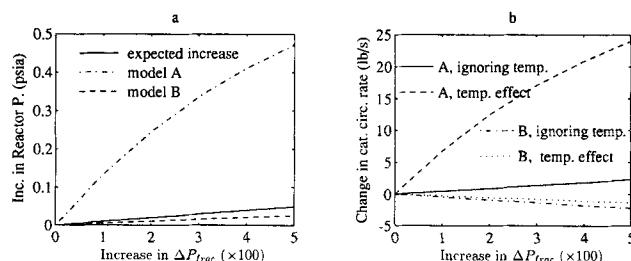


Figure 16. Effect of change in ΔP_{frac} on models A and B (full nonlinear models used).

expected for model B as predicted. Figure 16b shows the corresponding steady-state change in catalyst circulation rate. For each model the change in catalyst circulation rate is plotted as a function of the change in ΔP_{frac} when temperature effects are ignored and when temperature effects are taken into consideration. Note that for model A the increase in catalyst circulation rate for the actual process operation is much larger than if temperature effects were ignored, showing that the effect of the disturbance is amplified in model A. For model B the absolute change in catalyst circulation rate is lower in actual operation than when temperature effects are ignored.

Note from Figure 15 that for a given increase in reactor pressure, the absolute change in catalyst circulation rate is essentially the same for models A and B. Furthermore, the changes in catalyst circulation rate are proportional to changes in reactor pressure for both models. Figure 16a shows that there are larger changes in reactor pressure for model A than model B for identical disturbances (ΔP_{frac}) to the systems. Thus if one could independently control reactor pressure in model A and keep variation in reactor pressure small, then the fluctuations in catalyst circulation rates would be reduced for model A. It is common practice in industry to control reactor pressure by manipulating the wet-gas compressor throughput (Hovd and Skogestad, 1993; Lee and Groves Jr., 1985). Our quantitative arguments support this practice.

Important controlled variables like riser temperature and flue gas O_2 concentration are directly related to catalyst circulation rate. Changes in circulation rates lead to proportional changes in controlled variables (Figure 17). Increased catalyst flow for model A results in higher coke transport rate to the regenerator which consumes additional O_2 from the air supply and $C_{O_2,sg}$ decreases in the absence of any corrective action. Reactor temperature rises with increased regenerator temperature. Since catalyst circulation rate is lower for model B there is less coke being transported to the regenerator and less O_2 being consumed in combustion and $C_{O_2,sg}$ goes up. Reactor temperature decreases with regenerator temperature.

FCCU design objective

From the previous discussions the following design guidelines can be deduced so that FCCUs have low disturbance sensitivity. Ideally there should be no variations in catalyst

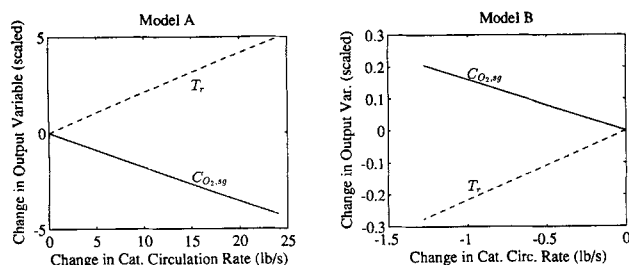


Figure 17. Relation between controlled variables and changes in catalyst circulation rate (nonlinear models).

circulation rate in the face of disturbances. In practice, the objectives should be

1. Design the FCCU so that the gain between changes in reactor pressure and changes in catalyst circulation rate at steady state is negative.
2. Design the FCCU flow system so that only small variations in catalyst flow rate occur when subjected to disturbances.

Most FCCUs have slide valves installed in the catalyst circulation lines to actively control catalyst circulation rate. The improvement in achievable performance when slide valves are installed in the catalyst U-bends of model B is now compared to the achievable performance of model B.

Installing Control Slide Valves in Catalyst Flow Lines

The main objective of using control slide valves in catalyst circulation lines is to control catalyst flow rates, but these are not available in model A or model B except for emergency closure in the event of catalyst flow reversal. Model IV FCCUs are sometimes refitted to incorporate slide valves that can be used to control catalyst circulation rate between the reactor and regenerator. This design modification was modeled and studied. The slide valve model used is described in detail in Appendix C. Slide valves were introduced into both the regenerated catalyst line and the spent catalyst line and were nominally 50% open. To regain some of the pressure drop across the slide valves it was necessary to implement the following *design* modifications as well (Figure 18).

1. Fresh feed inlet point was lowered from 124.5 to 118 ft (37.9 to 36.0 m).
2. Lift air inlet to standpipe was lowered from 134 to 98 ft (41 to 30 m).
3. Length of lift pipe was increased from 34 to 70 ft (10 to 21 m).
4. J-Bends were introduced to assist in feed oil and lift air entry.
5. Overall catalyst inventory was raised so that catalyst level in the regenerator was higher than the weir.

Thus the weir was flooded and the standpipe was operated so that it was always full [dense-bed height, 19.7 ft (6 m)] (this is an identical situation to model B).

The last modification was necessary since variations in pressure drop across the regenerated catalyst line result in large fluctuations in catalyst levels in the standpipe leading to occasional standpipe overflow. Such an overflow would result in significant process disturbances since process dynamics when the standpipe is not flooded and when it is flooded are considerably different. We will refer to the original model IV FCCU modified to incorporate slide valves and including modifications 1–5 above as *model C*. Model C has two additional manipulated variables, slide valve opening on regenerated and spent catalyst lines. An additional control scheme (scheme SIV) is therefore available (Table 5).

Open-loop analysis of model C

Figure 19 is a plot of the maximum and minimum singular values of the control schemes SII and SIV as a function of frequency. The maximum singular value of the disturbance transfer-function matrix is also plotted.

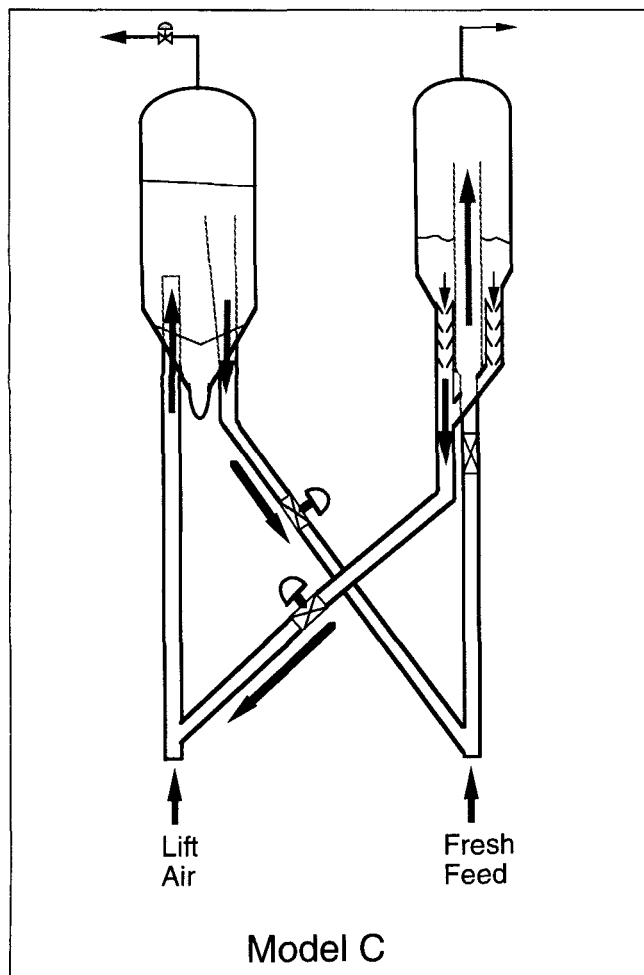


Figure 18. Design modification to model A—slide valves in catalyst flow lines.

The flow characteristics for model C are very similar to those of model B. In model C as in model B, an increase in reactor pressure results in decreased catalyst circulation rate at steady state (negative gain). The steady-state plant condition numbers as well as any RHPT zeros for model C schemes SII, and SIV are summarized in Table 6. Both control schemes have lower condition numbers than model A schemes. Scheme SIV has no RHPT zeros and should not have any inherent performance limitations. Scheme SII has an RHPT zero although it is outside the frequency range of interest.

It might be argued that if slide valves were installed to control catalyst flow rate that they would be used as manipulated variables and control schemes like SI, SII, and SIII would not be considered. The aim, however, is to compare model B modifications with model C modifications. In fact, model C, scheme II (in this case the slide valve openings were held constant) is identical to model B, scheme SII except for

Table 5. Additional Control Scheme for Model C

Notation	Controlled Variables	Manipulated Variables
SIV	$C_{O_2,sg}, T_r$	$V_{lift}, X_{su,rgc}$

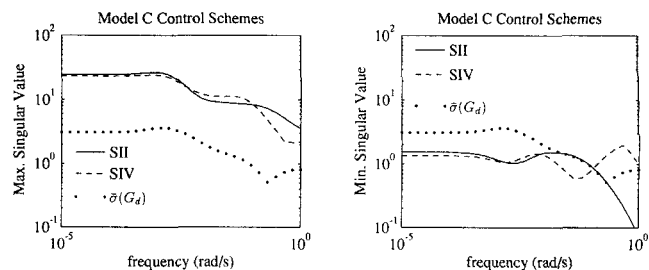


Figure 19. Frequency-response plots for disturbance model and schemes SII and SIV, model C.

the pressure drop across the J-bends which are not considered in model B and different cross-sectional areas for the slide valves.

Closed-loop analysis of model C

μ -Optimal controllers could be designed for model C schemes SII and SIV that guaranteed robust performance. Better robust performance, however, is achievable for model C scheme SIV (max. $\omega_p = 3.3$ rad/s) than for model C scheme SII (max. $\omega_p = 0.2$ rad/s). Recall that a higher value of ω_p implies faster closed-loop response. Model C scheme SIV should be expected to provide better closed-loop performance than model B schemes since the slide valves in scheme SIV can be used to directly and rapidly damp out variations in catalyst flow rate, which is not possible for model B schemes. To compare the improvement in achievable performance due to the introduction of slide valves the μ -plots for model C scheme SII and SIV are graphed in Figure 20 for identical uncertainty and performance conditions ($\omega_p = 0.2$ rad/s).

Figure 21 shows the closed-loop (nominal) response to a unit step in ΔP_{frac} for both SII and SIV. The deviations of controlled variables from setpoints are larger for scheme SII than for scheme SIV. The fluctuations in catalyst circulation rate are comparable. The manipulated variable moves required to reject the disturbance are well within bounds and have not been plotted.

Figure 20 and Figure 21 are essentially comparisons of models B and C since model C scheme SII is identical to model B scheme SII except for the differences mentioned earlier. Note, however, that in model B only a simple operational modification is needed, while model C would entail significant revamping of the model IV FCCU.

Manipulated Variable Saturation at the Regulatory Level

Tables 7 and 8 tabulate the largest individual disturbances that can be rejected (at steady state) by each control scheme

Table 6. Steady-State Plant Condition Number and Location of RHPT Zero for Model C Control Schemes

Scheme	Condition No.	RHPT Zero
SII	16.1	3.71
SIV	17.3	None

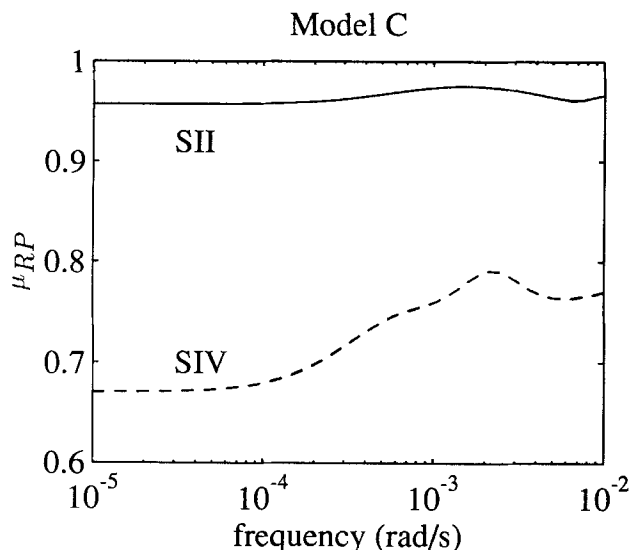


Figure 20. Robust performance comparison for schemes SII and SIV.

Identical uncertainty and performance specs. $\omega_p = 0.2$ rad/s.

for models A and B without saturating the manipulated variables. The corresponding manipulated variable moves required are also indicated. The disturbance condition number (Morari and Zafiriou, 1989; Skogestad and Morari, 1987) for each disturbance and each scheme is also tabulated. Tables 7 and 8 indicate that constraints are sometimes encountered in rejecting expected disturbances regardless of the configuration (model A or model B). Note, however, that in all cases

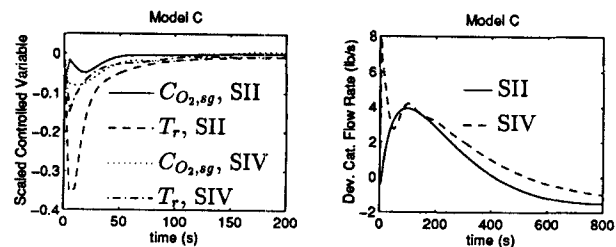


Figure 21. Closed-loop time response to a unit disturbance in ΔP_{frac} for model C, schemes SII and SIV, $\omega_p = 0.2$ rad/s.

the disturbance condition numbers are much smaller than the plant condition number, indicating that individual disturbances are closely aligned with the best disturbance direction. The best disturbance direction is the disturbance input direction requiring the *least* action by the manipulated variables. A disturbance input aligned exactly with the best direction has a disturbance condition number of 1.

Table 9 gives a singular value decomposition (SVD) (Eq. 21) of the steady-state gain matrix for the three control schemes in Table 6 for model A. Any significant RHPT zeros are also tabulated. Table 10 tabulates the corresponding values for model B.

$$G(0) = U\Sigma V^* \quad (21)$$

The maximum singular value of the plant gain matrix in schemes SI for both models A and B are significantly lower than the maximum singular value in schemes SII for models A and B. The manipulated variable combination in scheme

Table 7. Steady-State Process Variables Required for Disturbance Rejection in Model A Schemes

	SI			SII			SIII		
	d1	d2	d3	d1	d2	d3	d1	d2	d3
Max. Dist. Rej. max 1	1	0.3259	0.2394	1	1	1	1	1	1
Manip. Var.									
V_{14}	0	0	0	-0.0169	-0.0597	-0.0903	0	0	0
V_{lift}	0.8131	0.8685	0.8839	0.3026	0.2326	0.2759	0.4433	0.5431	0.7915
F_3	0.5451	1.0	1.0	0	0	0	0	0	0
T_2	0	0	0	0	0	0	-0.0238	-0.1501	-0.2089
Dist. Condt. No.	2.22	5.00	4.79	7.15	3.04	2.56	2.45	1.68	1.71
Plant Condt. No.	207	207	207	363	363	363	59.4	59.4	5.94

Table 8. Steady-State Process Variables Required for Disturbance Rejection in Model B Schemes

	SI			SII			SIII		
	d1	d2	d3	d1	d2	d3	d1	d2	d3
Max. Dist. Rej. max 1	1	0.8603	0.4639	1	1	1	1	1	0.6837
Manip. Var.									
$V_{14} (\times 10^3)$	0	0	0	8.636	49.9	-79.6	0	0	0
V_{lift}	0.3329	-0.7616	0.8033	0.4464	-0.2936	0.4885	0.0712	0.2306	-0.3083
F_3	-0.1654	-1.0	1.0	0	0	0	0	0	0
T_2	0	0	0	0	0	0	0.4884	-0.8170	1.0
Dist. Condt. No.	1.00	2.97	2.82	9.15	3.97	4.06	2.39	2.93	3.04
Plant Condt. No.	4.22	4.22	4.22	10.2	10.2	10.2	3.51	3.51	3.51

Table 9. Steady-State SVD Analysis and Plant RHPT Zeros, Model A Control Schemes

Scheme	U		Σ		V		Cond. No.	RHPT Zero
SI	0.663	0.749	92.8	0	0.871	-0.491	207	None
	-0.749	0.663	0	0.449	-0.491	-0.871		
SII	-0.635	-0.772	957	0	0.996	-0.084	363	0.273
	0.772	-0.635	0	2.64	-0.084	-0.996		
SIII	-0.627	-0.779	225	0	0.358	-0.934	59.4	None
	0.779	-0.627	0	3.80	-0.934	-0.358		

SI does not have a strong enough effect on the outputs to compensate for the effect of expected disturbances. This is also evident in the open-loop frequency-response plots for model A (Figure 4) and model B (Figure 11), where the maximum disturbance gain is often greater than the maximum plant gain. Note that scheme SIII, model B cannot compensate for expected disturbances in d_3 for a similar reason.

It is interesting to note that a plant input in the direction of high plant gain results in one output variable increasing while the other decreases for most control schemes, for example, for model A, scheme SI, an input along the direction $[0.871 \ 0.491]^T$ results in an increase in $C_{O_{2,sg}}$ and a decrease in T_r (Table 9). Thus relatively small control action is required to move both the controlled variables in opposite directions, but a large control action is required to move both in the same direction (increase both T_r and $C_{O_{2,sg}}$). This behavior can be physically justified. In the absence of any other energy source to heat up the riser, such as direct heating of the feed to the riser (control scheme SIII), an increase in riser temperature must result from an increase in regenerator temperature. An increase in regenerator temperature results from burning coke at a higher rate in the regenerator, requiring additional oxygen supply. In the absence of any control action, $C_{O_{2,sg}}$ would decrease.

Another interesting difference between models A and B is in the qualitative difference in behavior for scheme SIII. In model A scheme SIII, an input in the direction of large plant gain causes the outputs to move in opposite directions (Table 9), while in model B scheme SIII, the outputs move in the same direction for the equivalent input (Table 10). This observation is also physically justified.

For model A, scheme SIII, riser temperature could be raised by heating the feed to the FCCU. Higher riser temperature results in a higher wet-gas production rate and therefore an increase in reactor pressure. Since there is a *positive* gain between changes in reactor pressure and changes in catalyst circulation rate for model A, catalyst circulation rate would increase. The rate of coke transfer from the reactor to the regenerator would increase, requiring additional oxygen for combustion. In the absence of any control action, $C_{O_{2,sg}}$

would decrease. This is observed in Table 9, scheme SIII, where an input along the direction $[0.358 \ 0.934]^T$ results in a decrease in $C_{O_{2,sg}}$ and an increase in T_r .

For model B, scheme SIII, riser temperature could be raised by heating the feed to the FCCU. Higher riser temperature results in a higher wet-gas production rate and therefore an increase in reactor pressure. Since there is a *negative* gain between changes in reactor pressure and changes in catalyst circulation rate for model B, catalyst circulation rate would decrease. The rate of coke transfer from the reactor to the generator would decrease, requiring less oxygen for combustion. In the absence of any control action, $C_{O_{2,sg}}$ would increase. Thus both T_r and $C_{O_{2,sg}}$ would increase. This is observed in Table 10, scheme SIII, where an input along the direction $[0.891 \ 0.454]^T$ results in an increase in $C_{O_{2,sg}}$ and an increase in T_r .

Suppose it is desired to increase both T_r and $C_{O_{2,sg}}$. Increasing T_r is achieved by increasing the coke transport rate to the regenerator, resulting in reduced $C_{O_{2,sg}}$. The air supply has to be increased beyond what is needed to burn off the additional coke to increase $C_{O_{2,sg}}$. Thus large control action is required to increase both T_r and $C_{O_{2,sg}}$. The gain in this direction is therefore low. The arguments for scheme SII can be deduced from the last two paragraphs.

For completeness we tabulate the largest disturbances that can be rejected (at steady state) by each control scheme for model C and the corresponding manipulated variable moves required in Table 11. The SVD analysis of the steady-state gain matrix and RHPT zeros for control schemes SII and SIV, model C, is tabulated in Table 12. All the individual disturbances can be rejected with available control action.

Conclusions

The conventional setup of a model IV FCCU where a weir and standpipe arrangement is used in the regenerator section is found to be the source of the following undesirable characteristics in the FCCU process: high disturbance sensitivity—Disturbances result in large fluctuations of catalyst circulation rate leading to significant deviations in output

Table 10. Steady-State SVD Analysis and Plant RHPT Zeros, Model B Control Schemes

Scheme	U		Σ		V		Cond. No.	RHPT Zero
SI	-0.036	1.00	3.43	0	0.920	-0.391	4.22	2.860×10^{-3}
	1.00	0.036	0	0.81	-0.391	-0.920		
SII	0.866	-0.500	28.4	0	0.998	-0.067	10.2	$1.86 \pm i11.1$
	-0.500	-0.866	0	2.79	-0.067	0.998		
SIII	0.333	-0.943	6.72	0	0.891	-0.454	3.51	1.762×10^{-3}
	0.943	0.333	0	1.92	0.454	0.891		

Table 11. Steady-State Process Variables After Disturbance Rejection for Model C Schemes

	SII			SIV		
	d1	d2	d3	d1	d2	d3
Max. Dist. Rej. max 1	1	1	1	1	1	1
Manip. Var. $V_{14} (\times 10^3)$	-0.34	85.8	-63.3	0	0	0
V_{lift}	0.1777	-0.6863	0.7274	0.3592	-0.110	-0.0174
$X_{v,rgc} (\times 10^3)$	0	0	0	-7.69	-99.7	85.4
Dist. Condt. No.	16.1	7.16	9.30	16.7	1.43	1.03
Plant Condt. No.	16.1	16.1	16.1	17.3	17.3	17.3

variables from setpoint; plant directionality—The plant is ill-conditioned.

Operating the conventional model IV FCCU with the weir and standpipe flooded at all times leads to a significant reduction in disturbance sensitivity and better control.

The installation of control slide valves in catalyst J-bends is found to improve closed-loop performance over both the original model IV FCCU and the FCCU modified to operate with the weir flooded.

The most significant disturbances to FCCU operation were found to be variations in feed coking characteristics and variations in reactor pressure. One can attempt to minimize fluctuations in reactor pressure and therefore reduce the effect of reactor pressure disturbances. Our analysis corroborates the common industrial practice of maintaining reactor pressure at setpoint by manipulating wet-gas compressor throughput. However, since the coking characteristics of the feed to the FCCU are not known accurately, variations in coking characteristics cannot be avoided in practice.

The control objective at the regulatory level was to reject expected disturbances and maintain flue gas O_2 concentration ($C_{O_2,sg}$) and riser temperature (T_r) at prespecified setpoints. Two manipulated variables were selected from a set of available manipulated variables to achieve this objective. The other manipulated variables were maintained at their nominal values. Using fresh feed rate (F_3) and lift air supply (V_{lift}) as manipulated variables resulted in plant gains that were too low to reject the expected disturbances at steady state. Manipulating lift air supply (V_{lift}) and flue gas valve position (V_{14}), however, resulted in significantly higher plant gains, and therefore provided effective disturbance rejection for all FCCU designs considered. For the standard model IV FCCU, feed temperature (T_2) and lift air supply (V_{lift}) were also found to be effective manipulated variables in rejecting expected disturbances. Incorporating slide valves to control the catalyst circulation rate through the FCCU provided an additional effective manipulated variable when used in conjunction with lift air supply at the regulatory level.

Based on this study the following design guidelines for low

disturbance sensitivity have been established for FCCUs. The FCCU flow system should be designed so that increased reactor pressure results in decreased catalyst circulation rate. The FCCU should be designed so that catalyst circulation rates are minimally affected by changes in process conditions.

This study is based on the FCCU reactor/regenerator model developed by McFarlane et al. (1993). We considered only the regulatory level of the control hierarchy; overall process optimization was not addressed. The emphasis was on understanding those aspects (both design and operational) of model IV FCCUs that render them difficult to control. The aim was not to design controllers for actual model IV FCCUs based on this model. Instead, controllers were designed for similar performance and stability objectives to compare alternate operating modes and different possible design modifications to the model IV FCCU. Based on our observations we identified some desirable characteristics of FCCUs that make control easier.

It must be stressed that the findings reported in this article for the original model IV FCCU are based on the assumption that the underlying nonlinear model adopted from McFarlane et al. (1993) captures the dynamic characteristics of model IV FCCU operation with a reasonable degree of accuracy.

We have explicitly considered process constraints in this analysis except to the extent of determining the largest individual disturbances that can be rejected at steady state. Industrial experience indicates that constraints are effectively handled at higher levels of the control hierarchy (above the regulatory level). The focus of this work was at the regulatory level, and process constraints were not considered in the analysis.

Our linear analysis strictly applies to a narrow region around the operating point described. The dynamic characteristics of the FCCU, however, are qualitatively the same as long as the FCCU is operated under total combustion mode (Arbel et al., 1993). Therefore, the results are generally valid for FCCU operation in the total combustion mode.

Table 12. Steady-State SVD Analysis and Plant RHPT Zeros, Model C Control Schemes

Scheme	U		Σ		V		Condition No.	RHPT Zero
SII	0.967	-0.254	24.8	0	1.00	-0.001	16.1	3.71
	-0.254	-0.967	0	1.54	-0.001	-1.00		
SIV	-0.741	0.672	23.3	0	0.04	1.00	17.3	None
	0.672	0.741	0	1.35	1.00	-0.04		

Acknowledgments

Financial support from Chevron Research and Technology Company is gratefully acknowledged. We would also like to thank Serban Agachi, John Bomberger, and Bruno Donno for their help with this project. Finally, we thank Professor Reuel Shinnar for some enlightening discussions.

Notation

- A_i = cross-sectional area of unit i , ft² (m²)
 \hat{d} = nondimensional input disturbance
 E_{lift} = elevation of regenerator lift air injection, ft (m)
 E_{oil} = elevation where oil enters reactor riser, ft (m)
 F_{reg} = regenerated catalyst flow rate, lb/s (g/s)
 F_{sp} = catalyst flow rate over weir, lb/s (g/s)
 g_c = Newton's law proportionality constant (32 ft·lb_m/lb_f·s²)
 h_{lift} = height of lift pipe (ft)
 T_{atm} = ambient temperature (°F)
 T_{reg} = regenerator temperature, °F (°C)
 \bar{U} = left-singular vectors of $G(0)$
 \bar{V} = right-singular vectors of $G(0)$
 V_6 = combustion air-blower suction-valve position (0-1)
 V_{11} = wet-gas compressor suction-valve position (0-1)
 W_p = diagonal matrix of performance weights, diag (w_p)
 z_{bed} = regenerator dense-bed height, ft (m)

Greek letters

- ΔW_i = catalyst inventory change in unit i , lb (kg)
 ψ_F = effective coke factor for gas-oil feed

Literature Cited

- Arbel, A., Z. Huang, I. H. Rinard, and R. Shinnar, "Partial Control of FCC Units: Input Multiplicities and Control Structures," AICHE Meeting, St. Louis, MO (1993).
 Balas, G. J., J. C. Doyle, K. Glover, A. Packard, and R. Smith, *μ -Analysis and Synthesis Toolbox, Users Guide*, The Math Works, New York (1991).
 Elnashaie, S. S. E. H., and I. M. El-Hennawi, "Multiplicity of the Steady State in Fluidized Bed Reactors: IV. Fluid Catalytic Cracking (FCC)," *Chem. Eng. Sci.*, **34**, 1113 (1979).
 Elnashaie, S. S. E. H., and S. S. Elshishini, "Digital Simulation of Industrial Fluid Catalytic Cracking Units: IV. Dynamic Behavior," *Chem. Eng. Sci.*, **48**(3), 567 (1992).
 Felipe, L. I., "Dynamic Modeling of an Industrial Fluid Catalytic Cracking Unit," *Proc. Eur. Symp. on Computer Aided Process Engineering: I. Escape I*, Elsinore, Denmark, p. S139 (1992).
 Grosdidier, P., A. Mason, A. Aitolahti, P. Heinonen, and V. Vanhamäki, "FCC Unit Reactor-Regenerator Control," *Comp. Chem. Eng.*, **17**(2), 165 (1993).
 Holt, B. R., and M. Morari, "Design of Resilient Processing Plants—VI. The Effect of Right-Half-Plane Zeros on Dynamic Resilience," *Chem. Eng. Sci.*, **40**(1), 59 (1985).
 Hovd, M., and S. Skogestad, "Procedure for Regulatory Control Structure Selection with Application to the FCC Process," *AICHE J.*, **39**(12), 1938 (1993).
 Kalra, L., J. F. Bartee, and C. Georgakis, "On the Use of the Amoco FCCU Model in a Graduate Process Control Class," AICHE Meeting, St. Louis, MO (1993).
 Kurihara, H., "Optimal Control of Fluid Catalytic Cracking Processes," PhD Thesis, MIT, Cambridge, MA (1967).
 Lee, E., and F. R. Groves, Jr., "Mathematical Modeling of the Fluidized Bed Catalytic Cracking Plant," *Trans. Soc. Comp. Simul.*, **2**(3), 219 (1985).
 Lundström, P., S. Skogestad, and Z. Wang, "Performance Weight Selection for H-Infinity and μ -Control Methods," *Trans. Inst. of Measurement & Control*, **13**(5), 241 (1991).
 McFarlane, R. C., R. C. Reineman, J. F. Bartee, and C. Georgakis, "Dynamic Simulator for a Model IV Fluid Catalytic Cracking Unit," *Comp. Chem. Eng.*, **17**(3), 275 (1993).
 Monge, J. J., and C. Georgakis, "Multivariable Control of Catalytic Cracking Processes," *Chem. Eng. Commun.*, **61**(1-6), 197 (1987).
 Morari, M., and E. Zafiriou, *Robust Process Control*, Prentice-Hall, Englewood Cliffs, NJ (1989).
 Morari, M., E. Zafiriou, and B. R. Holt, "Design of Resilient Processing Plants—New Characterization of the Effect of RHP Zeros," *Chem. Eng. Sci.*, **42**(10), 2425 (1987).
 Skogestad, S., and M. Morari, "Effect of Disturbance Directions on Closed Loop Performance," *Ind. Eng. Chem. Res.*, **26**(10), 2029 (1987).
 Skogestad, S., M. Morari, and J. C. Doyle, "Robust Control of Ill-Conditioned Plants: High-Purity Distillation," *IEEE Trans. Automat. Contr.*, **AC-33**(12), 1092 (1988).

Appendix A: Steady-State Operating Points

Independent Variables. The nominal values of the independent variables for models A, B, and C are tabulated in Table 13.

Disturbances. The nominal values of the process disturbances for models A, B, and C are tabulated in Table 14.

Output Variables. The nominal values of the output variables for models A, B, and C are tabulated in Table 15.

Comparison of Linear and Nonlinear Models: Model A. The agreement between the linear and nonlinear models is good within the time scales of interest (minutes to hours), as Figure 22 shows.

For model A there are significant differences between the linear and nonlinear models at steady state, as Figure 23 shows.

Comparison of Linear and Nonlinear Models: Model B. There is no discernible difference between the linear and nonlinear models for model B within the resolution of the plot (Figure 24).

Table 13. Steady-State Operating Points (Independent Variables)

Variable	Units	Model A	Model B	Model C	Scale Factor
V_{11}	%	93.94	93.94	89.6	10
V_{14}	%	61.23	65.0	61.23	14
V_{lift}	%	48.61	56.0	60.0	60
V_6	%	100.0	95.0	100.0	—
E_{lift}	ft	134.0	134.0	98.0	—
h_{lift}	ft	34.0	34.0	70.0	—
E_{oil}	ft	124.5	124.5	118.0	—
F_3	lb/s	130.0	130.0	126.0	1.8
T_2	°F	661.0	661.0	661.0	50
$X_{\text{sv,reg}}$	%	N/A	N/A	50.0	25
$X_{\text{sv,reg}}$	%	N/A	N/A	50.0	25

Table 14. Steady-State Operating Points (Disturbances)

Variable	Units	Model A	Model B	Model C	Scale Factor
T_{atm}	°F	75	75	75	25
ψ_F	—	1	1	1	0.025
ΔP_{frac}	psia	9.5	9.5	9.5	0.5

Table 15. Steady-State Operating Points (Output Variables)

Variable	Units	Model A	Model B	Model C	Scale Factor
T_r	°F	991.5	993.4	990.8	1
T_{reg}	°F	1,275.2	1,274.6	1,265.9	10
$C_{\text{O}_2, \text{sg}}$	mol %	1.395	2.11	1.99	0.15
F_{reg}	lb/s	750.4	768.2	739.2	—

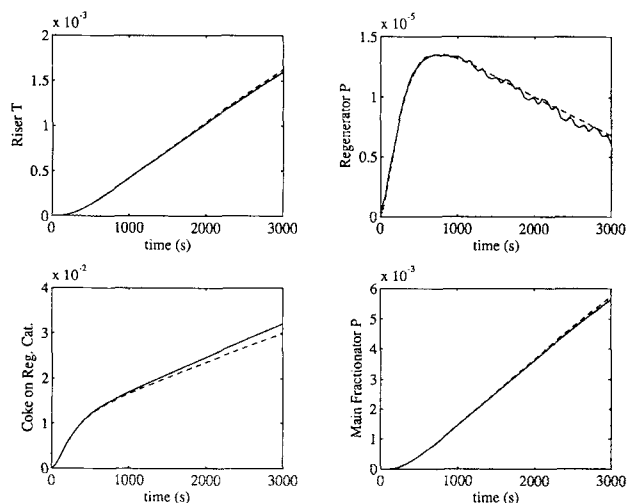


Figure 22. Open-loop step response of linear and nonlinear models to 0.2 (scaled) step in ψ_t , model A (dynamic characteristic).

Nonlinear model (solid), linear model (dashed).

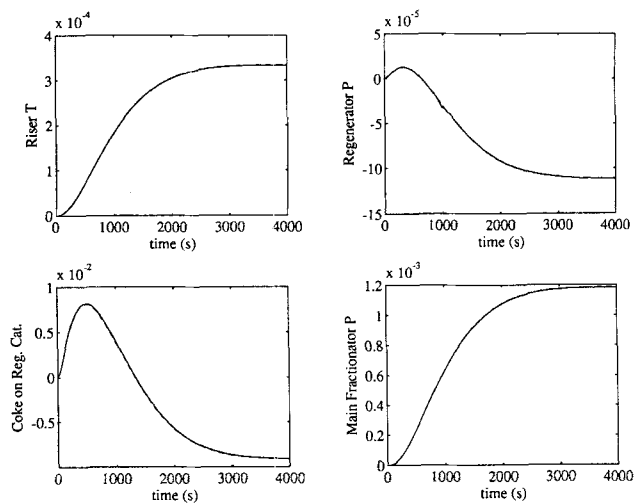


Figure 24. Open-loop step response of linear and nonlinear models to 0.2 (scaled) step in ψ_t , model B.

Nonlinear model (solid), linear model (dashed).

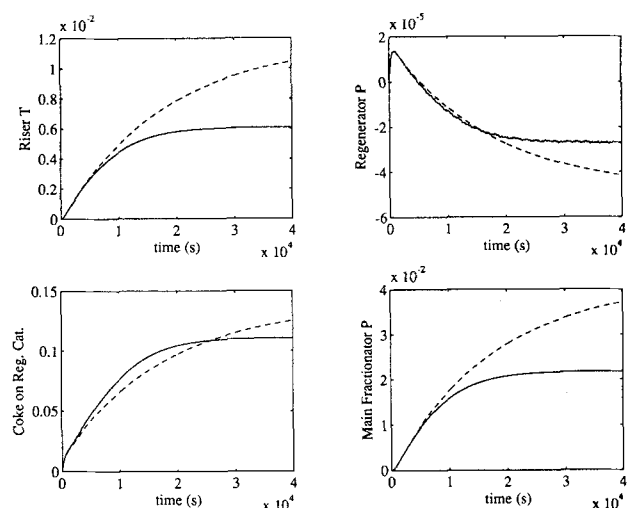


Figure 23. Open-loop step response of linear and nonlinear models to 0.2 (scaled) step in ψ_t , model A (steady-state characteristic).

Nonlinear model (solid), linear model (dashed).

Appendix B: Linear State Space Models for Selected Control Schemes

State-space realizations for selected control schemes are given below. Note that the matrices are written as follows:

$$A = A_p = A_d; \quad B = [B_p \quad B_d];$$

$$C = C_p = C_d; \quad D = [D_p \quad D_d] \quad (22)$$

where subscript p refers to the plant matrices and subscript

d refers to the disturbance matrices. The linear time-invariant model of the system is given by

$$\dot{x} = Ax + [B_p \quad B_d] \begin{bmatrix} u \\ d \end{bmatrix} \quad (23)$$

$$y = Cx + [D_p \quad D_d] \begin{bmatrix} u \\ d \end{bmatrix} \quad (24)$$

where

u = vector of manipulated variables
 y = vector of output variables
 d = vector of disturbances
 x = vector of system states

The plant transfer function matrix is given by

$$G(s) = C(sI - A)^{-1}B_p + D_p \quad (25)$$

and the disturbance transfer function matrix is given by

$$G_d(s) = C(sI - A)^{-1}B_d + D_d. \quad (26)$$

The input and output vectors are specified individually for each model. The disturbances are always the same, namely $d^T = [d_1 \quad d_2 \quad d_3]$.

The states do not have an obvious physical interpretation, as the model dimension was reduced after linearization. The original linear system was balanced and the Hankel singular values examined to determine truncation order. The balanced system was then truncated, yielding the reduced-order linear model. This procedure is described by Balas et al. (1991).

Model A, SH

$$u^T = [V_{14} \quad V_{\text{lift}}], \quad y^T = [C_{\text{O}_2, \text{sg}} \quad T_r] \quad (27)$$

$$A = \begin{bmatrix} -0.0001 & -0.0004 & -0.0003 & 0.0007 & -0.0002 & 0.0002 & -0.0005 & 0.0009 \\ -0.0007 & -0.0269 & -0.0236 & 0.0872 & -0.0080 & -0.0140 & -0.0167 & -0.0134 \\ 0.0003 & 0.0376 & -0.0076 & -0.0136 & -0.0079 & 0.0210 & -0.0244 & 0.0612 \\ -0.0009 & -0.0877 & 0.0457 & -0.0930 & 0.0334 & 0.0294 & 0.0913 & -0.0465 \\ 0.0001 & 0.0081 & -0.0037 & 0.0017 & -0.0202 & 0.0214 & -0.0949 & 0.1519 \\ -0.0004 & -0.0327 & 0.0207 & -0.0938 & 0.0685 & -0.2335 & 0.3998 & -0.9782 \\ -0.0002 & -0.0050 & 0.0050 & -0.0547 & -0.0380 & -0.1174 & -0.3890 & 0.6133 \\ -0.0001 & -0.0237 & 0.0140 & -0.0059 & 0.1768 & -0.2759 & 1.2183 & -2.8816 \end{bmatrix}$$

$$B_p = \begin{bmatrix} 0.2499 & -0.0210 \\ 1.3762 & 0.1207 \\ -0.5825 & -0.0554 \\ 1.4988 & -0.2019 \\ -0.1563 & -0.2848 \\ 0.8178 & 0.4819 \\ 0.2352 & -0.9369 \\ 0.4094 & 2.2000 \end{bmatrix} \quad B_d = \begin{bmatrix} 0.0106 & 0.0188 & 0.0281 \\ -0.0346 & 0.0004 & -0.0436 \\ 0.0193 & 0.0089 & 0.0167 \\ 0.0643 & 0.0027 & 0.1882 \\ 0.1052 & -0.0192 & 0.1613 \\ -0.1461 & 0.0015 & -0.0248 \\ 0.3442 & 0.0245 & -0.0197 \\ -0.8543 & 0.0162 & 0.0284 \end{bmatrix}$$

$$C = \begin{bmatrix} -0.1618 & 0.2508 & -0.5771 & 0.1987 & -0.2902 & 0.9296 & -0.8348 & 2.3944 \\ 0.1948 & 1.3596 & 0.1001 & -1.5123 & 0.2424 & 0.2427 & 0.5964 & -0.0740 \end{bmatrix}$$

$$D_p = \begin{bmatrix} 1.8199 & 0 \\ 0 & 0 \end{bmatrix} \quad D_d = \begin{bmatrix} 0 & 0 & -0.1216 \\ 0 & 0 & 0 \end{bmatrix}.$$

Model B, SH

$$u^T = [V_{14} \quad V_{\text{lift}}], \quad y^T = [C_{\text{O}_2, \text{sg}} \quad T_r] \quad (28)$$

$$A = \begin{bmatrix} -0.0035 & 0.0092 & -0.0032 & 0.0123 & -0.0465 & 0.0292 & -0.0055 & 0.0002 \\ 0.0129 & -0.0492 & -0.0040 & 0.0318 & 0.1659 & -0.1372 & 0.0170 & -0.0062 \\ -0.0032 & 0.0275 & -0.0038 & 0.0146 & -0.0796 & 0.0504 & -0.0099 & 0.0001 \\ 0.0192 & -0.1224 & 0.0308 & -0.2208 & 0.6949 & -0.3665 & 0.1113 & 0.0195 \\ -0.0114 & 0.0138 & -0.0154 & 0.3274 & -2.2601 & 1.4896 & -0.4788 & -0.0259 \\ -0.0030 & 0.0485 & -0.0069 & -0.0675 & 1.1214 & -0.8382 & 0.2524 & -0.0106 \\ 0.0017 & -0.0124 & 0.0029 & -0.0099 & -0.2406 & 0.2245 & -0.1109 & -0.0155 \\ -0.0009 & 0.0038 & -0.0018 & 0.0251 & -0.1379 & 0.0792 & -0.0249 & -0.0202 \end{bmatrix}$$

$$B_p = \begin{bmatrix} -0.3246 & -0.0047 \\ 0.7858 & 0.0867 \\ -0.2083 & -0.0187 \\ 1.0241 & 0.4649 \\ -0.6821 & -2.0687 \\ -0.0708 & 1.1937 \\ 0.0913 & -0.1700 \\ -0.0426 & -0.0538 \end{bmatrix} \quad B_d = \begin{bmatrix} 0.0050 & 0.0286 & -0.0303 \\ 0.0375 & 0.0039 & 0.1917 \\ 0.0122 & 0.0026 & -0.0034 \\ -0.2096 & 0.0113 & -0.1478 \\ 1.0602 & 0.0085 & 0.0453 \\ -0.6677 & 0.0153 & 0.0571 \\ 0.2095 & 0.0161 & -0.0943 \\ 0.0399 & 0.0102 & 0.0121 \end{bmatrix}$$

$$C = \begin{bmatrix} -0.3028 & 0.4836 & -0.2019 & 1.0281 & -2.4224 & 1.3256 & -0.2960 & -0.0213 \\ 0.1241 & -0.6553 & 0.0563 & 0.5233 & -0.0554 & -0.3493 & -0.0516 & -0.0781 \end{bmatrix}$$

$$D_p = \begin{bmatrix} 1.5331 & 0 \\ 0 & 0 \end{bmatrix} \quad D_d = \begin{bmatrix} 0 & 0 & -0.1337 \\ 0 & 0 & 0 \end{bmatrix}.$$

Model C, SH

$$u^T = [V_{14} \quad V_{\text{lift}}], \quad y^T = [C_{\text{O}_2, \text{sg}} \quad T_r] \quad (29)$$

$$A = \begin{bmatrix} -0.0080 & 0.0430 & -0.0016 & 0.0285 & -0.0994 & 0.0109 & -0.0025 \\ 0.0401 & -0.2928 & 0.0211 & -0.2419 & 0.9900 & -0.1192 & 0.0256 \\ -0.0009 & -0.0015 & -0.0004 & 0.0108 & -0.0362 & 0.0041 & -0.0009 \\ 0.0191 & -0.2015 & 0.0055 & -0.3034 & 0.8857 & -0.0878 & 0.0189 \\ -0.0087 & 0.1342 & -0.0111 & 0.7297 & -2.9679 & 0.4821 & -0.1727 \\ -0.0076 & 0.0696 & -0.0013 & 0.0011 & 0.1511 & -0.0624 & 0.0428 \\ 0.0008 & -0.0131 & 0.0006 & -0.0324 & 0.1602 & -0.0247 & -0.0133 \end{bmatrix}$$

$$B_p = \begin{bmatrix} 0.4087 & 0.0379 \\ -1.3925 & -0.4805 \\ 0.0355 & 0.0268 \\ -0.5353 & -0.7414 \\ 0.2471 & 2.4259 \\ 0.2013 & -0.1932 \\ -0.0107 & -0.0630 \end{bmatrix} \quad B_d = \begin{bmatrix} -0.0147 & -0.0353 & 0.0065 \\ 0.1365 & -0.0126 & -0.0224 \\ -0.0033 & 0.0087 & 0.0215 \\ 0.2538 & -0.0060 & 0.2186 \\ -0.9284 & -0.0054 & 0.0437 \\ 0.1317 & -0.0043 & -0.0161 \\ -0.0217 & 0.0528 & -0.0059 \end{bmatrix}$$

$$C = \begin{bmatrix} 0.4094 & -1.4734 & 0.0503 & -0.8679 & 2.6079 & -0.2498 & 0.0566 \\ -0.0484 & 0.1346 & 0.0010 & -0.4417 & -0.0944 & 0.1819 & -0.0647 \end{bmatrix}$$

$$D_p = \begin{bmatrix} 1.1564 & 0 \\ 0 & 0 \end{bmatrix} \quad D_d = \begin{bmatrix} 0 & 0 & -0.0748 \\ 0 & 0 & 0 \end{bmatrix}.$$

Model C, SIV

$$u^T = [V_{\text{lift}} \quad X_{sv,rgc}], \quad y^T = [C_{O_2,sg} \quad T_r] \quad (30)$$

$$A = \begin{bmatrix} -0.0037 & -0.0052 & -0.0005 & 0.0486 & 0.0032 & -0.0028 & 0.0004 \\ -0.0214 & -0.0851 & 0.0065 & -0.0513 & 0.0165 & -0.0179 & 0.0321 \\ -0.0006 & -0.0101 & -0.0002 & 0.0251 & 0.0011 & -0.0006 & -0.0007 \\ -0.0028 & -0.0437 & -0.0053 & -3.5030 & -0.7640 & 0.5424 & 0.5007 \\ -0.0021 & -0.0162 & -0.0011 & 0.6300 & -0.0073 & 0.0543 & 0.0050 \\ 0.0001 & 0.0014 & -0.0002 & -0.5614 & -0.0483 & -0.0085 & 0.0287 \\ -0.0046 & -0.0360 & -0.0013 & -0.2978 & -0.0119 & -0.0257 & -0.0355 \end{bmatrix}$$

$$B_p = \begin{bmatrix} 0.0061 & -0.3041 \\ -0.1058 & -0.9887 \\ 0.0013 & -0.0337 \\ -2.6860 & -0.0022 \\ -0.0003 & -0.0839 \\ -0.0846 & -0.0082 \\ -0.0410 & -0.1885 \end{bmatrix} \quad B_d = \begin{bmatrix} -0.0057 & -0.0328 & 0.0122 \\ 0.0303 & 0.0054 & 0.1082 \\ -0.0034 & -0.0041 & -0.0129 \\ 0.9951 & -0.0019 & 0.0072 \\ 0.0600 & 0.0166 & -0.0650 \\ -0.0453 & 0.0041 & -0.0745 \\ -0.0647 & -0.0091 & 0.0365 \end{bmatrix}$$

$$C = \begin{bmatrix} 0.2108 & -0.1366 & 0.0352 & -2.8641 & -0.0814 & 0.0484 & 0.1439 \\ -0.2221 & -0.9913 & -0.0097 & 0.0385 & 0.0923 & -0.1118 & 0.1487 \end{bmatrix}$$

$$D_p = \begin{bmatrix} 0 & 0 \\ 0 & 0 \end{bmatrix} \quad D_d = \begin{bmatrix} 0 & 0 & -0.0748 \\ 0 & 0 & 0 \end{bmatrix}.$$

Appendix C: Slide-Valve Model

The pressure drop across each slide valve is given by

$$\Delta P_{sv} = \left[\frac{50 F_{\text{cat}}}{K A_{sv} X_{sv}} \right]^2 \frac{1}{\rho_c} \quad (31)$$

where

F_{cat} = catalyst flow rate, ton/min

K = dimensional constant, 0.7

A_{sv} = open area of slide valve, 213 in.²

X_{sv} = fractional opening of slide valve

ρ_c = settled catalyst density, 45 lb/ft³

The pressure drop across each J-bend is given by:

$$\Delta P_{elb} = \frac{1}{2} N \rho_c v^2 \quad (32)$$

where

N = number of velocity heads, 20

ρ_c = settled catalyst density, 45 lb/ft³

v = velocity through J-bend, ft/s

Manuscript received Mar. 10, 1994, and revision received July 20, 1994.